OAK RIDGE NATIONAL LABORATORY
MANAGED BY UT-BATTELLE FOR THE US DEPARTMENT OF ENERGY

Predictive model for swelling accumulation in austenitic steels under light water reactor relevant conditions

Stanislav I. Golubov[1], Alexander V. Barashev[1,2]
[1]Oak Ridge National Laboratory
[2]University of Tennessee

Light Water Reactor Sustainability Program:

Performance Milestone M2LW-17OR0402042

August 2017

Evaluation of Swelling Effects in High-Fluence Core Internals Work Package

Under the Light Water Reactor Sustainability Program

Predictive model for swelling accumulation in austenitic steels under conditions relevant to light water reactor

Stanislav I. Golubov[1], Alexander V. Barashev[1,2]

[1]Materials Science and Technology Division Oak Ridge National Laboratory Oak Ridge, TN 37831-6114, USA

[2]Center for Materials Processing Department of Materials Science and Engineering University of Tennessee, Knoxville, TN 37996-0750, USA

Prepared for:

Light Water Reactor Sustainability Program Office of Nuclear Energy, Science and Technology U.S. Department of Energy

August 2017
Oak Ridge National Laboratory

ABSTRACT

A mean-field, cluster dynamics model of the microstructure evolution in austenitic steels of light water reactors which reproduces the incubation period of swelling has been developed for the first time. In agreement with observations, it predicts that, although the void nucleation starts from the very beginning of irradiation, their growth beyond certain, relatively small size, is delayed until the onset of the transient period of swelling. Such a delayed growth of voids is explained by the interaction of voids randomly distributed over the volume with one-dimensionally migrating clusters of self-interstitial atoms, which are produced in cascades of atomic displacements. The incubation period of swelling is followed by the transient stage, when voids start to grow with increasing rate due to development of the experimentally-observed spatial correlations between voids and extended defects, such as second-phase precipitates and dislocations, which screen voids from the mobile clusters. A critical role of residual gas on void nucleation, which diminishes importance of He atoms from transmutation reactions, is revealed.

1. INTRODUCTION

Since the discovery of void swelling in materials under irradiation [1], most measurements have been performed for fast and experimental sodium-cooled reactors in the temperature range from 350 to 650°C. The temperature and neutron fluence dependences of the existing database imply that there should be no significant swelling below 350°C. This is in agreement with the predictions of the BEK model [2] which assumes formation of either vacancy loops or stacking fault tetrahedra below ~0.3 of the melting temperature. However, the void growth has been reported even below 300°C (see, e.g. [3-7]), which is a contradiction.

The data for light water reactor (LWR) internal components have been analyzed using the cluster dynamic approach for irradiation doses of up to 100 dpa to make predictions of the material performance for extended reactor operations (see, e.g. [8-12]). Although the results showed reasonable agreement with some of the data, the assumptions of the model seem questionable. First, the calculations have been performed in the framework of the model, which accounts for the three-dimensionally (3-D) migrating single vacancies and self-interstitial atoms (SIAs), but ignores the defect clustering in displacement cascades and one-dimensional (1-D) migration of the SIA clusters produced by cascades, as revealed in molecular dynamics studies (see, e.g. [13]) and experiments. Second, the simulations assume random spatial distribution of voids, which contradicts observations that, at high irradiation doses, the voids are correlated with, e.g. secondary phase precipitate particles, as in the pioneering work by Cawthorne and Fulton [1]. A detailed study by Kozlov *et al*. [14] demonstrated that the main contribution to swelling at high irradiation doses comes from voids associated with secondary phase precipitates and, especially, dislocations. In addition, we note that the gas-assistant void nucleation is one of the key processes in the present context, but has not been treated rigorously due to the absence of a comprehensive mathematical

description and appropriate integration methods.

For these reason, explanation of the incubation stage of swelling, which lasts for up to 50 dpa depending on the temperature (see, e.g. [15]), proposed in [8-12] is incorrect. So, the low swelling levels during this stage, is attributed in [8-12] to difficulty of void nucleation, which contradicts observations and theory. The void densities measured in [4] show (see Fig. 1) that voids nucleated long before the onset of the transient stage (~50 dpa). The void mean diameter reaches ~10 - 20 nm already at very low irradiation doses (see Fig. 2), but does not increase further with increasing dose. Note that the smaller void sizes at higher irradiation doses in Fig. 2 correspond to lower temperatures (see Fig. 3), when vacancy loops are highly stable and slow down the void growth by increasing the total sink strength for migrating defects. So, Figs. 1 and 2 cannot be considered as strictly dose dependences, since the data points correspond to different temperatures. From this we conclude that low swelling levels during the incubation stage are due to the absence of void growth rather than problems in void nucleation. Such a behavior is in agreement with the predictions of the Production Bias model (PBM) [16, 17], which takes into account both the 3-D migrating point defects and 1-D migrating SIA clusters. According to the model, the voids form at the very beginning of irradiation because of high vacancy super-saturation, due to in-cascade clustering of SIAs, and negligibly small interaction cross-section of small voids with 1-D migrating SIA clusters. For growing voids, which are randomly distributed over the volume, the cross-section of interaction with 1-D migrating clusters increases faster than that for 3-D migrating vacancies. As a result, voids cannot grow larger than $4\pi r_d$ in diameter for randomly distributed voids and two times larger this value for void screened by precipitates (ppts), where r_d is the capture radius of dislocations for the SIA clusters (see [16] for details). The value of r_d is ~1 nm (see text related to Fig. 6 in [18]), hence maximum void diameter, d_{max}, is ~10 nm for randomly distributed voids and 20 nm for voids screened by ppts, which agrees well with the data in Fig. 2. One may conclude that spatial distribution of voids within the irradiation doses in ref [4] must be random or screened by ppts, which is in agreement with the data in [15], where the duration of the incubation dose of swelling at 400°C is ~ 50 dpa.

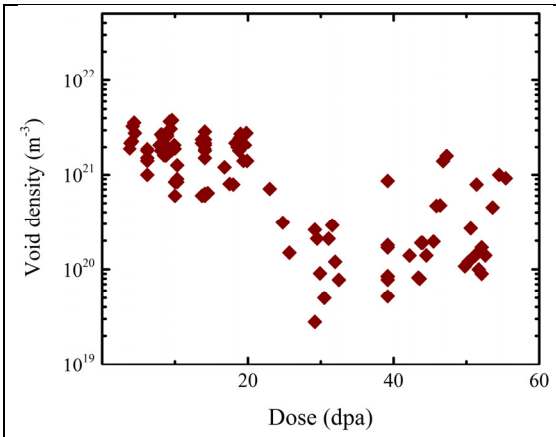

Fig. 1. Dose dependence of void density measured in AISI 321 type of steel [4].

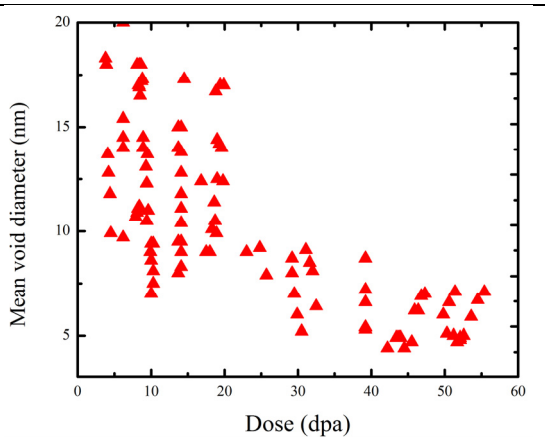

Fig. 2. Dose dependence of void size measured in AISI 321 type of steel [4].

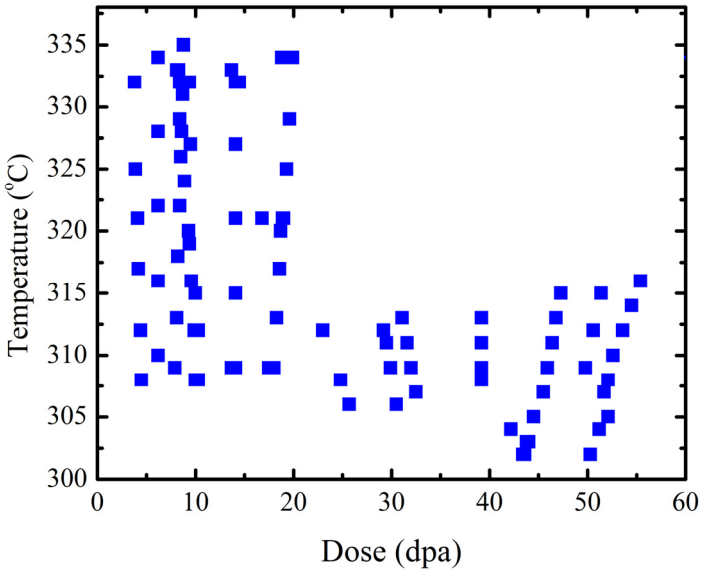

Fig. 3. Dose dependence of temperatures for void densities and sizes in Figs. 1 and 2.

In the PBM, the incubation stage takes place at random distribution of voids with the maximal size ~10 nm and voids screened by ppts with the maximum size ~20 nm. The transient stage of swelling starts due to development of spatial correlations between voids and dislocations. As derived in [16], for the microstructure consisting of voids, ppts and dislocations (including prismatic loops of vacancy and interstitial type) the swelling rate is described by the following equation

$$\frac{dS}{d\phi} = \left(1-\varepsilon_r\right)\varepsilon_i^g \left(\frac{4\pi rN}{4\pi rN+\rho} - \frac{\eta(\phi)\pi r^2 N}{\eta(\phi)\pi r^2 N + \pi\rho r_d/2} \right), \qquad (1)$$

where ε_r and ε_i^g are the fractions of radiation produced defects recombined in cascades relative to the NRT standard value and of the SIAs produced in the form of 1-D migrating clusters, respectively; r, N, ρ are the mean void radius, void density and dislocation density, respectively; $\eta(\phi)$ is the correlation-screening factor, which is equal to unity in the absence of spatial correlations, 0.5 for voids screened by ppts and zero for voids screened by dislocations from 1-D mobile SIA clusters. Note that the dislocation bias due to stronger interaction of a dislocation with an SIA than a vacancy is accounted for in the calculations below but omitted here for simplicity, for it is not as crucial in the case of neutron irradiation as the production bias due to cascade-produced 1-D mobile SIA clusters (see estimates in [16]). The first term in the brackets of Eq. (1) is the probability of a 3-D migrating point defect to be absorbed by a void, which is equal to the ratio of the interaction cross-section of voids ($4\pi rN$) to the total cross-section given by the Smoluchowski equation. The second term is the same probability for 1-D migrating SIAs, in which case the interaction cross-section with voids is $\pi r^2 N$ (see [17]). After the incubation stage, development of spatial correlations of voids with dislocations leads first to partial screening of voids from SIA clusters $\eta(\phi) < 0.5$ hence swelling increase. At

high enough doses, voids become fully screened, $\eta(\phi) \to 0$, the second term in Eq. (1) becomes negligible, and the swelling rate reaches its maximum given by the first term:

$$\frac{dS}{d\phi} = \left(1-\varepsilon_r\right)\varepsilon_i^g \frac{4\pi rN}{4\pi rN+\rho} \approx \frac{1}{2}\left(1-\varepsilon_r\right)\varepsilon_i^g , \tag{2}$$

where in the last equation it is assumed that the sink strengths for voids and dislocation for 3-D migrating defects are equal, $4\pi rN \sim \rho$, as frequently reported.

Experimental data on swelling in BN-600 for temperatures 450-560°C in Fig. 4 (Fig. 2 in [14]) support the explanation of swelling stages proposed above, showing that c-type voids are the smallest and their size is about 10 nm, as predicted by the theory.

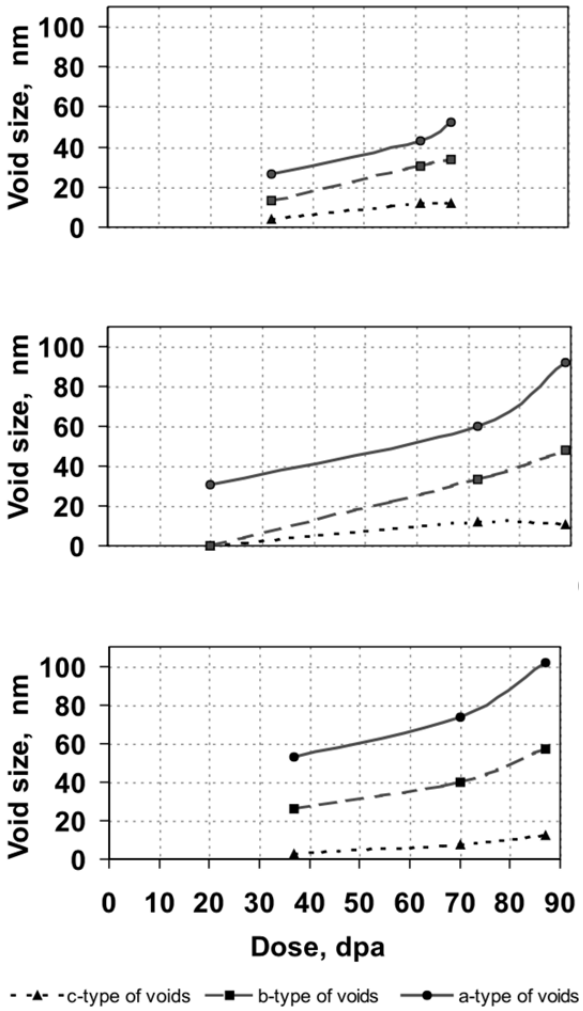

Fig. 4. Dose dependence of average size of different type voids at temperatures 450–480 °C, 500–510 °C and 550–560 °C. a-type voids are associated with dislocations, b-type with ppts; c-type voids are not associated with any defects.

Experimental data in [19] were obtained in BN-600 for Fe–18Cr–9Ni steel (analogous to AISI 304L) irradiated at 370°C ,and provide another confirmation of the theory predictions. Indeed, Table 1 in [19] show that void concentration reaches

saturation at ~1.7 dpa, whereas the void size reaches 10 nm, as in the theory for randomly distributed voids. In the dose range of 1.7-20.5 dpa the void size increases to 20 nm, as predicted for voids screened by ppts. Moreover, the size distribution of voids and corresponding microstructures found in [19] and shown in Figs. 5-8 demonstrate absence of ppts at small dose and their presence at high doses.

Table 1. Average sizes and densities of voids for doses 1.7-20.5 dpa (see Table 4 in [18]).

Lot #	Damage dose (dpa)	Average size of voids (nm)	Concentration of voids (10^{21} m^{-3})	Swelling (%)
1	1.7	10	4.1	0.25
2	9.9	13	5.2	1.00
3	12.4	14	5.0	0.95
4	16.2	17	4.1	1.60
5	20.5	19	5.8	2.30

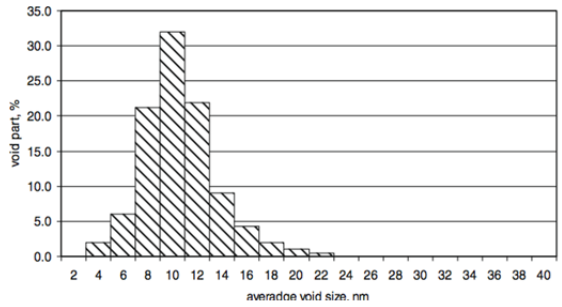

Fig. 5. Void size distribution at irradiation dose 1.7 dpa (Fig. 5a from [18]).

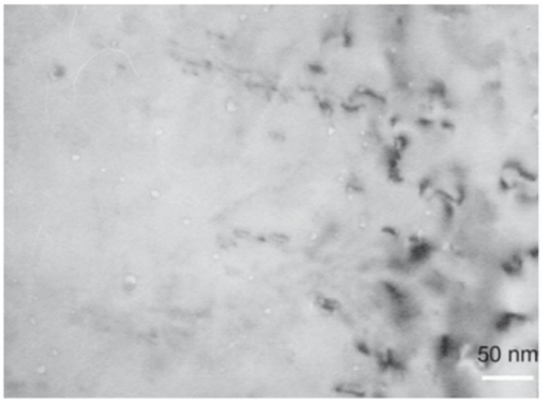

Fig. 6. Microstructure after at irradiation dose 1.7 dpa (Fig. 5b from [18]). Note absence of precipitates.

Below we present modeling results on swelling found in [4] and [18] using the RIME code (Radiation Induced Microstructure Evolution) [20], which uses grouping method for numerical integration of Master Equations (ME) [21-23] for voids filled with gas, and SIA and vacancy- dislocation loops taking into account 3-D migration of point defects and 1-D migration of SIA clusters. Brief description of the model incorporated in RIME code are given in Section 2. The calculation results and conclusions are presented in Sections 3 and 4.

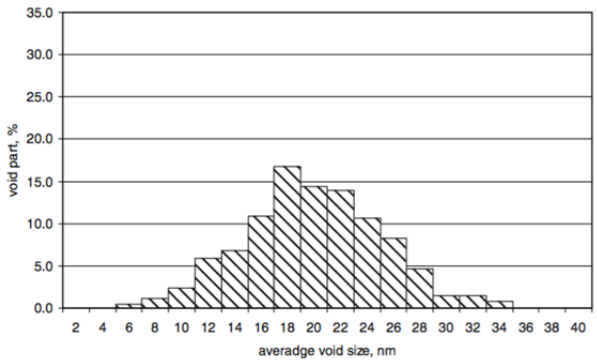

Fig. 7. Void size distribution at irradiation dose 20.5 dpa (Fig. 5f from [18]).

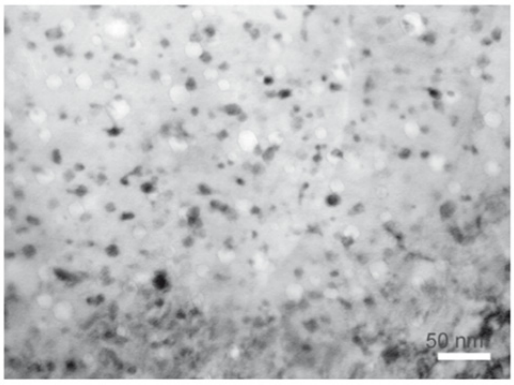

Fig. 8. Microstructure at irradiation dose 20.5 dpa (Fig. 5h from [18]). Note coexistance of voids and ppts.

2. COMPUTATIONAL MODEL

The RIME code [20] represents the rate theory description of the radiation damage, and calculates nucleation and growth of voids and vacancy- and interstitial-type dislocation loops during irradiation. The following features are taken into consideration.

1. The initial damage is produced in the form of point defects and their clusters in cascades of atomic displacements.
2. Vacancy clusters are assumed to be immobile, whereas the SIA clusters may be either immobile or migrate 1-D.
3. Existence of residual gas and its generation via transmutation reactions.
4. Transformation of dislocation loops into the dislocation network.
5. Evolution of dislocation density driven by radiation-induced climb, recombination of dislocations, and formation of new dislocations from prizmatic loops.
6. Development of spatial correlations between voids and dislocations and secondary phase particles.
7. Impurity atoms immobilize 1-D mobile SIA clusters that may grow into loops.

In the mean-field approach, an accurate description of an ensemble od voids containing gas atoms requires solution of two-dimensional ME for the size distribution (SD) of voids (cavities), $f_c(x,m,t)$, in a phase space defined by the variables x and m, the numbers of vacancies and gas (Helium) atoms in a cluster (cavity), respectively. The cluster of size x,m can change its size by absorption or emission of single vacancies, SIAs, gas atoms and 1-D migrating SIA clusters. The ME has the form

$$\frac{df(x,m,t)}{dt} = \left[J_x(x-1,m,\phi) - J_x(x,m,\phi) \right] + \left[J_m(x,m-1,\phi) - J_m(x,m,\phi) \right], \qquad (3)$$

where the fluxes of cavities in x, m space are

$$J_x(x,m,\phi) = P_x(x,m,\phi) f_c(x,m,\phi) - \left[Q_x(x+1,m,\phi) + Q_x^{cl}(x+1,m,\phi) \right] f_c(x+1,m,\phi) ,$$
$$J_m(x,m,\phi) = P_m(x,m,\phi) f_c(x,m,\phi) - Q_m(x,m+1,\phi) f_c(x,m+1,\phi) . \quad (4)$$

The coefficients $P_x(x,m,\phi)$, $Q_x(x,m,\phi)$ and $Q_x^{cl}(x,m,\phi)$ in (3) are the reaction rates between cavities and 3-D migrating vacancies, SIAs and 1-D migrating SIA clusters, respectively; $P_m(x,m,\phi)$ and $Q_m(x,m,\phi)$ are the capture and emission rates for gas atoms, ϕ is irradiation dose. The emission of vacancies from cavities is accounted for in the $Q_x(x,t)$ term. Explicit expressions for these can be found, e.g. in [20-22]. The size distributions of vacancy- and interstitial-type dislocation loops are described in the RIME code by similar one-dimensional equations.

Numerical integration of Eqs. (3) for practically important irradiation doses is unrealistic, since the number of equations is too large, ~10^{12}. A grouping method developed in [21, 22] is based on approximation of the size distributions of cavities by a linear function within a group of sizes Δx_i and Δm_j:

$$f_c^{i,j}(x,m) = L_0^{i,j} + L_{1x}^{i,j}(x - < x >_i) + L_{1m}^{i,j}(m - < m >_j) , \quad (5)$$

where $<x>_i$ and $<m>_j$ are the mean numbers of vacancies and gas atoms in the group. This method reduces the number of equations in a group from $\Delta x_i * \Delta m_j$ to three and the total number of equation to ~10^4. Such an approach provides approximate solution of Eq. (3), with reasonable accuracy for the two important measurable integrals of the cavity population: the density of cavities and the number of point defects in cavities.

It is well known that residual gas in material under irradiation plays an important role in cavity nucleation, but it has never been rigorously accounted for in the models. In the RIME code, the residual gas atoms is in the form of gas-vacancy complexes of concentration C_g, and is accounted for in the initial condition for the void size distribution

$$f_c(1,1,0) = C_g . \quad (6)$$

Gas atoms increase thermal stability of cavities, hence facilitate cavity nucleation. For simplicity, we assume the residual gas to be helium (He), the same as generated by neutrons in transmutation reactions. In this case, the equation of state for gas bubbles, as a function of gas density $n=m/x$, is given by

$$p = Z(n) n k_B T , \quad (7)$$

which is needed to determine the vacancy and gas atom emission rates from a cavity. The compressibility factor, Z, in Eq. (7) is defined as in Carnahan-Starling model [23]:

$$Z(n) = \begin{cases} \dfrac{1 + y + y^2 - y^3}{(1-y)^3}, & y < 0.5, \\ Z = a \ln(nb - c), & y \geq 0.5, \end{cases} \quad (8)$$

with a smooth extrapolation for y>0.5 to avoid irregularities for y approaching unity. Here $y = \pi n \sigma^3 / 6\Omega$ is the packing fraction, Ω the atomic volume, σ=2 nm the hard sphere diameter, and a, b, and c are equal to 33.97, 1.87 and 0.42, respectively [24].

The spatial correlations between voids, ppts and dislocations are accounted for with the RIME code as follows

$$\eta(\phi)=\begin{cases}1, & \phi\le\phi_1\\ 1-\frac{1}{2}\left(\frac{\phi-\phi_1}{\phi_2-\phi_1}\right)^{n_1}, & \phi_1<\phi\le\phi_2,\\ \frac{1}{2}, & \phi_2<\phi\le\phi_3,\\ \frac{1}{2}\left[1-\left(\frac{\phi-\phi_3}{\phi_4-\phi_3}\right)^{n_2}\right], & \phi_3<\phi\le\phi_4,\\ 0, & \phi>\phi_4\ ,\end{cases} \tag{9}$$

where doses ϕ_1 and ϕ_2 correspond to the beginning and end of void screening by ppts whereas doses ϕ_3 and ϕ_4 correspond to the beginning (coincides with the end of the incubation stage) and end of screening by dislocations (which corresponds to the beginning of the steady state stage). The temperature dependences of ϕ_3 and ϕ_4 at temperatures >400°C are shown in Fig. 9, which are deduced from experimental data in Fig. 10. The dotted line in Fig. 9 shows possible range of the steady state doses below 400°C where experimental data are absent. Due to absence of the data < 400°C, it is assumed in the calculations below that the doses ϕ_3 and ϕ_4 are equal to those at 400°C, which probably underestimates their values hence overestimates swelling accumulation, hence giving its upperbound at high doses.

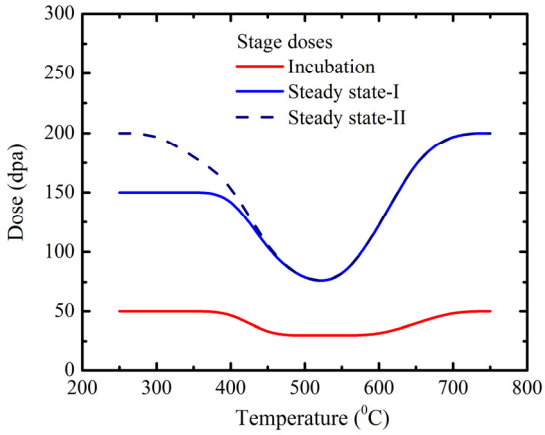

Fig. 9. Incubation and steady state doses deduced from the data in Fig. 10. The dotted line shows possible range of the steady state doses at temperatures below 400°C.

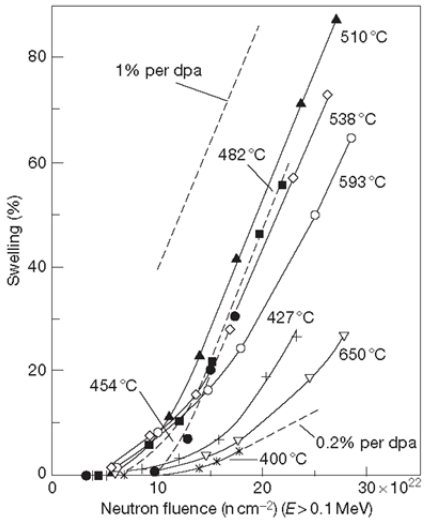

Fig. 10. Dose dependence of swelling in stainless steels at temperature 400-650°C [15].

3. CALCULATION RESULTS

Experimental data on swelling for LWR internal components and fast breeder reactors (FBRs) at LWR relevant conditions are presented in a review by Chung [6] and show wide scatter of void densities and mean sizes. The swelling measured, e.g. in [4] at 302-329°C and in [19] at 370°C show void densities from 10^{20} to 5×10^{21} m^{-3} and void sizes from 5 to 20 nm (see Figs. 1 and 2). Qualitatively different data were obtained in [25] for similar temperatures 290-320°C, where extremely high void densities were found, ~10^{24} m^{-3}, but the voids were small, ~1 nm. In our view, the reaction kinetics responsible for swelling in experiments performed in [4] and [25] are qualitatively different. Such conclusion comes from comparison with theory predictions. The theory predicts saturation of void size at 10-20 nm for voids distributed randomly or associated with ppts due to competition in absorption of 3-D migrating defects with 1-D migrating SIA clusters by voids. The void sizes found in [4] and [18] are in the range predicted by the theory, whereas those found in [25] contradict it. The reasons for such behavior in the later case are unknown and the main objective of this work is analysis of the results obtained in [4] and [18].

In Section 3.1, the effects of residual gas and irradiation-produced He atoms on void nucleation are considered since it is the key process determining void density. The modeling results are presented in Section 3.2. The main set of parameters used in calculation is listed in Table 1. The parameters determine stability of small vacancy-He clusters, which are crucial for nucleation and hence the terminal void density, as well as the void growth. The cascade parameters, i.e. the fractions of single and clustered defects, and the dislocation bias were taken from ref. [26]. Other parameters are taken from ref. [9,10,12], where experimental data on swelling in stainless steels irradiated with neutrons, similar to those under consideration, was studied.

Table 1. Input parameters for RIME code

Parameter	Value	Description
γ	1.65 J/m^2	Surface energy
E_v^f	1.8eV	Vacancy formation energy
E_v^m	1.2eV	Vacancy migration energy
E_{He}^m	0.3eV	He migration energy
D_{v0}	5.0×10^{-6} m^2/s	Pre-exponential factor in vacancy diffusion coefficient
D_{i0}	1.0×10^{-7} m^2/s	Pre-exponential factor in SIA diffusion coefficient
D_{g0}	1.0×10^{-6} m^2/s	Pre-exponential factor in He atom diffusion coefficient
ρ_d	1×10^{14}-2×10^{15} m^{-2}	Initial network dislocation density
B_d	0.04	Dislocation bias
ε_r	0.9	Fraction of defects recombined in cascades
ε_v	0.1	Fraction of vacancies produced in cascades as loops
ε_i^s	0.1	Fraction of SIAs produced in cascades as prismatic loops
ε_i^g	0.1	Fraction of SIAs produced as 1-D mobile clusters
$E_{2\mathrm{V}}$	0.3eV	Di-vacancy binding energy
r_d	1 nm	Interaction radius of a dislocation with an SIA cluster

3.1. Effect of residual gas on void nucleation

There are numerous experimental data shown that minor concentrations of gas atoms, such as hydrogen and oxygen, play an important role in void nucleation in pure metal and alloys including stainless steels (see, e.g. [27] and [28] and reference therein). Theoretical study of the gas effect on void nucleation has a long history, which also came to similar conclusion. However, the gas assisted void nucleation has never been taken into account rigorously in numerous works devoted to modeling of swelling accumulation since it could be done numerically only by solving two-dimensional ME for gas filled voids. The reason for this is related to extremely high number of equations, which have to be solved (~10^{12}) in order to account for the effect of gas atoms on void nucleation. The groping method developed by us [20, 21], which is realized in the RIME code, for the first time provides a method to solve the problem. An example of microstructure evolution, i.e. evolution of voids, SIA and vacancy loops in the case of 100 appm/dpa generation rate of He in the absence of residual gas obtained by RIME at

300°C is preseneted in Figs. 11. Note that the size distribution of voids, $f(x,m,t)$, is connected with the size distribution $f(R,\phi)$ preseneted in Figs. 11 as

$$f(R,t)=\sum_{m}F(R,m,t)\,, \tag{10}$$

where

$$F(R,m,t)=\left(\frac{36\pi}{\Omega}\right)x^{2/3}f(x,m,t)\,, \tag{11}$$

where R and Ω in Eq. (11) are the void radius and atomic volume. The two-dimensional size distribution, $F(R,m,t)$, at doses of 1 and 50 dpa are shown in Figs. 12 and 13 (*Ln m* is the logarithm of the mean number of gas atoms in a void at different sizes of voids).

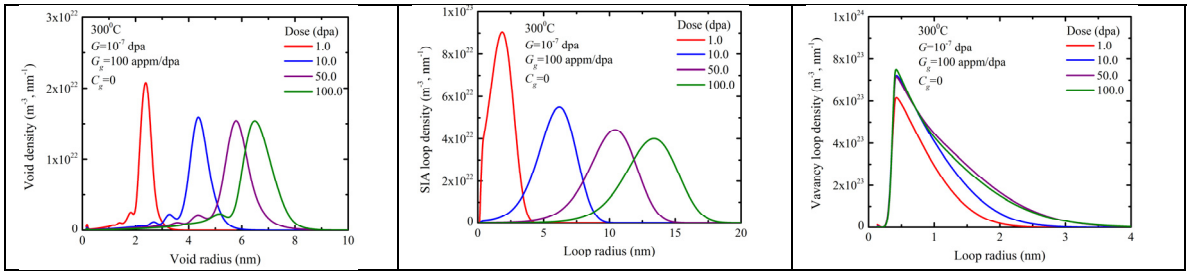

Figs. 11. Evolution of voids, SIA loops and vacancy loops at 100 appm/dpa generation rate of He in the absence of residual gas.

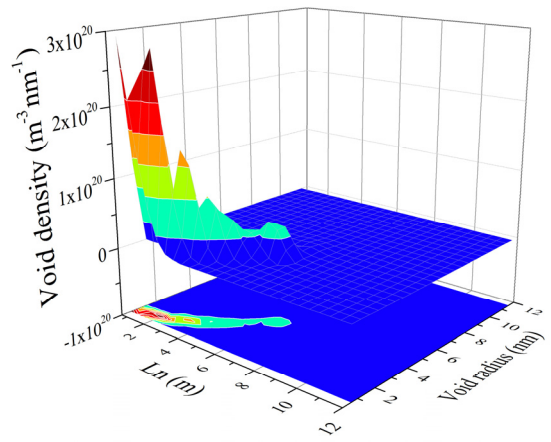

Fig. 12. Size distributions of voids at 300°C after 1 dpa irradiation at 100 appm/dpa He atom generation rate in the absence of residual gas.

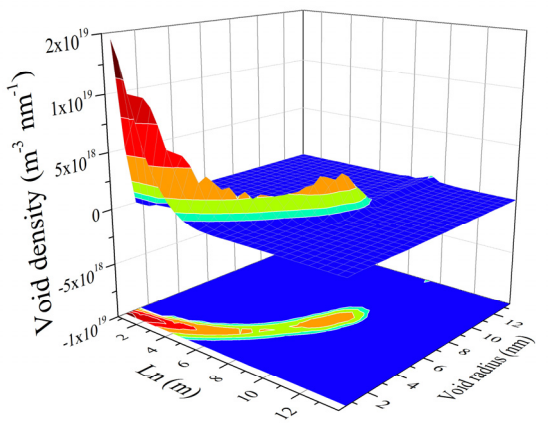

Fig. 13. Size distributions of voids at 300°C after 50 dpa irradiation at 100 appm/dpa He atom generation rate in the absence of residual gas.

Swelling at FBR conditions in the temperature range of 275-600°C for irradiation up to 100 dpa was calculated by RIME either in the presence of residual gas (Fig. 14) or for radiation-produced He (Fig. 15). It has been found that in both cases the temperature of the maximum swelling is ~500°C and variation of swelling with temperature is similar

to that observed in [15]. But the effect of gas atoms on void nucleation and growth is different. So, at 100 dpa, the same level of maximum swelling is observed for 1 appm of residual gas and 100 appm/dpa generation rate, when the total accumulated He at 100 dpa is 10^4 appm. In addition, in the presence of residual gas, voids are nucleated over a wider range of temperatures than when gas is produced during irradiation. This large scatter of void densities in a narrow temperature range observed in [4] may be due to fluctuations of residual gas concentrations in different areas of irradiated samples.

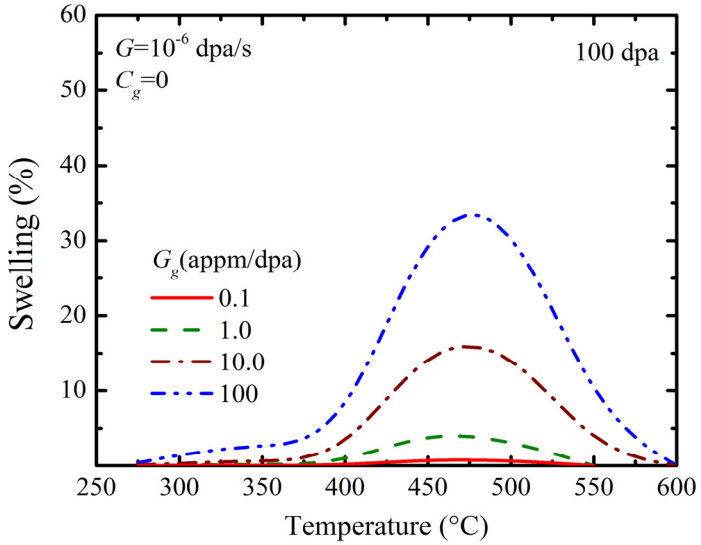

Fig. 14. Temperature dependence of swelling at 100 dpa calculated by RIME code for different generation rates of He atoms in the absence of residual gas.

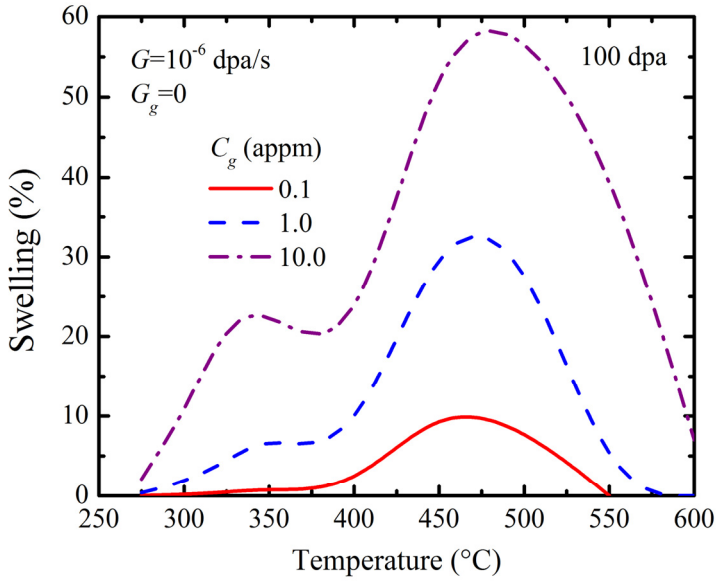

Fig. 15. Temperature dependence of swelling at 100 dpa calculated by RIME code for different levels of residual gas concentrations in the absence of He atom production by irradiation.

The results of calculations presented in Figs. 12, 13 and 16, where the size distributions of voids obtained in the range of 50 dpa at two different cases are presented, explain why residual gas is more efficient for void nucleation. In the case when gas is produced during irradiation (Figs. 12 and 13) the gas atoms are distributed over a wide range of void sizes. Importantly, the number of gas atoms in small voids, which participated in nucleation, is small, hence, a large number of He atoms generated do not participate in void nucleation, but join large already stable voids. This is qualitatively different from the case when void nucleation takes place in the presence of residual gas, as shown in Fig. 16. In this case, a high density of voids containing small number of gas atoms necessary for nucleation are formed at the very beginning of irradiation, and the number of gas atoms per void does not change during irradiation. In other words, residual gas atoms are all used almost exclusively for void nucleation, whereas the radiation-produced He are captured by large already stable voids. Note also that the calculated dose dependences of swelling at 400 and 500°C presented in Fig. 17, which are obtained at 1 appm concentration of residual gas, show good correlation with experimental data in [15].

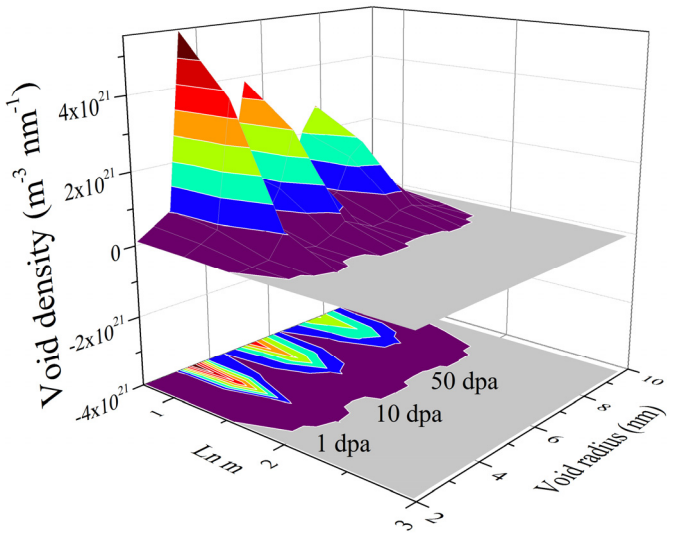

Fig. 16. Size distributions of voids at 300°C at three different irradiation doses calculated for residual gas concentration of 1 appm, in the absence of He atom generation.

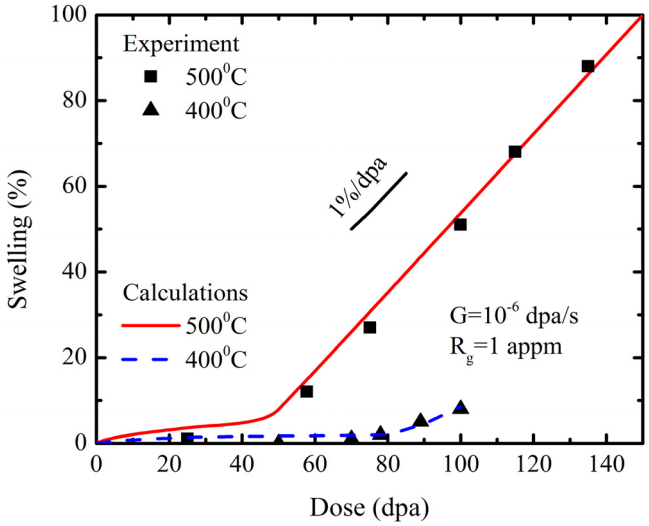

Fig. 17. Comparison of the RIME code calculations accounting for 1 appm residual gas with experimental results on swelling in SS 316 irradiated in FBR reactor [15].

3.2. Swelling accumulation at LWR conditions

Swelling data presented in [4] and [19] are obtained in the temperature range of 300-370°C, i.e. at temperatures below those in fast breeder reactor [15] shown in Fig. 10. It will be shown below that the data in [4] and [19] may be considered as a continuation of data in [15] to low temperatures despite the damage rates in [4], [19] are an order, or even more, smaller than in [15]. Moreover, the data, which represent swelling behavior within the incubation stage, provide more detail information taking place at this stage.

The data in [4] are obtained in the temperature range of 302-335°C presented in Figs.18-21 together with the results obtained by RIME provide a unique opportunity to see two qualitative different behavior of swelling accumulation. Indeed, the mean size of voids in the temperature range of 302-315°C is significantly smaller than 10 nm in the dose range up to ~50 dpa than that predicted by the theory, whereas it is ~20 nm already at much low doses. Swelling accumulation in the low temperature range agreed well with the predictions of the model [2] which assumes formation of either vacancy loops or stacking fault tetrahedra at temperatures below ~0.3 of the melting temperature. The calculation results presented in Figs. 18 and 19, which are in reasonable agreement with the experimental data, correspond to the case when vacancy loops are the strongest sink for mobile defects that suppresses the voids growth. For example, their sink strength for 3-D migrating defects is two times larger than that of SIA loops and about three orders of magnitude larger than that of voids. Our calculations show that variation of the void sizes measured at the low temperatures shown in Fig. 18 takes place mainly due to variation in the void densities, which comes from the difference in residual gas concentrations. Note also that swelling remains very low at doses ~100 dpa and above (not show here), which does not depend from the initial value of dislocation density.

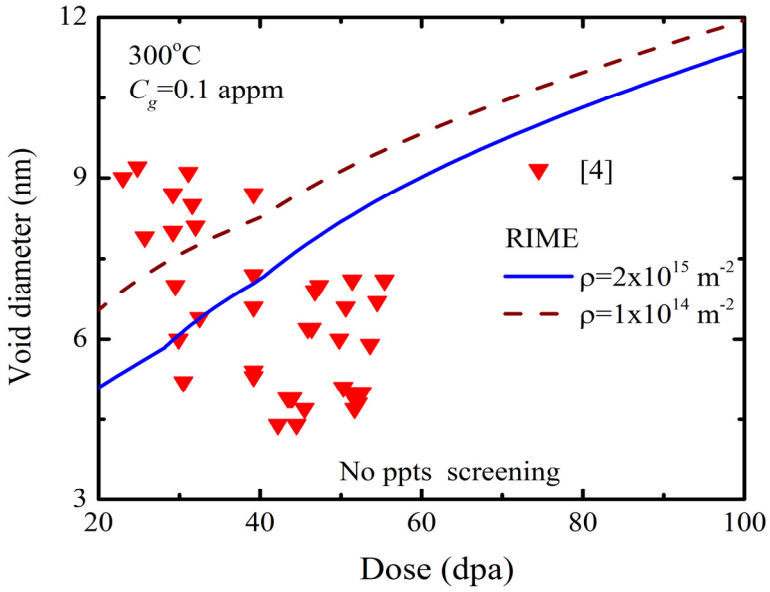

Fig. 18. Comparison of dose dependence of void size at 300°C calculated with RIME code with those measured in the temperature range of 302-315°C in [4].

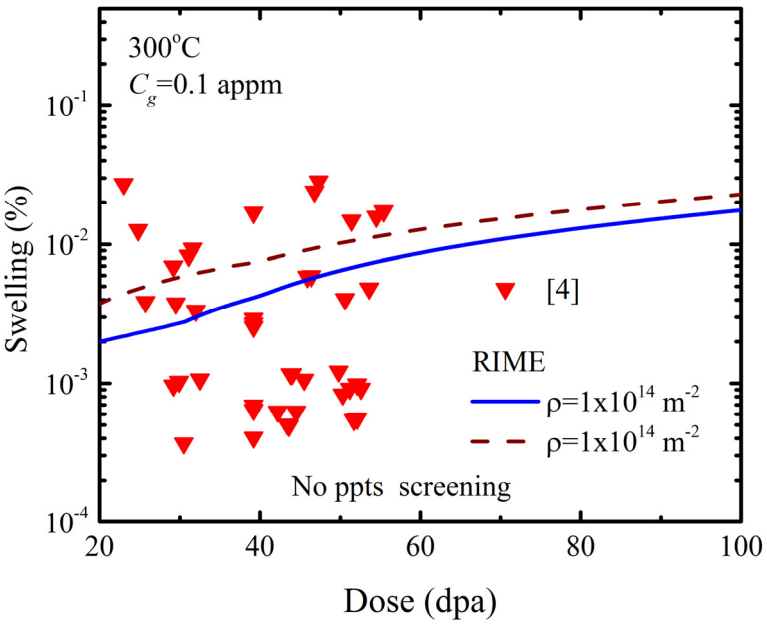

Fig. 19. Comparison of dose dependence of swelling at 300°C calculated with RIME code with those measured in the temperature range of 302-315°C in [4].

Swelling accumulation at temperatures above 315°C shown in Figs. 20 and 21 is qualitatively different as compared to that at low temperatures. In this case the void sizes are reached 10-20 nm at doses ~3-5 dpa and do not grow until ~20 dpa at least. Such void evolution agrees fully with theory predictions that the size of randomly distributed voids is ~10 nm, whereas it is ~20 nm for voids spatially correlated with ppts, which is the case as can be seen on Fig. 5 in [4]. In the calculations presented in Figs. 20 and 21

the doses ϕ_1 and ϕ_2 in Eq. (9) are taken to be equal to 5 and 12 nm, respectively, that is the reason why swelling rate increased at doses larger than 12 dpa. Swelling accumulation in this case (see Fig. 21) is higher than that at low temperatures reaching ~ several percent at 100 dpa. Such an increase takes place for two reasons: higher void density and smaller effect of vacancy loops, as compared to those at low temperatures. Note that the calculation results show that the initial value of dislocation density does not play any role at this temperature.

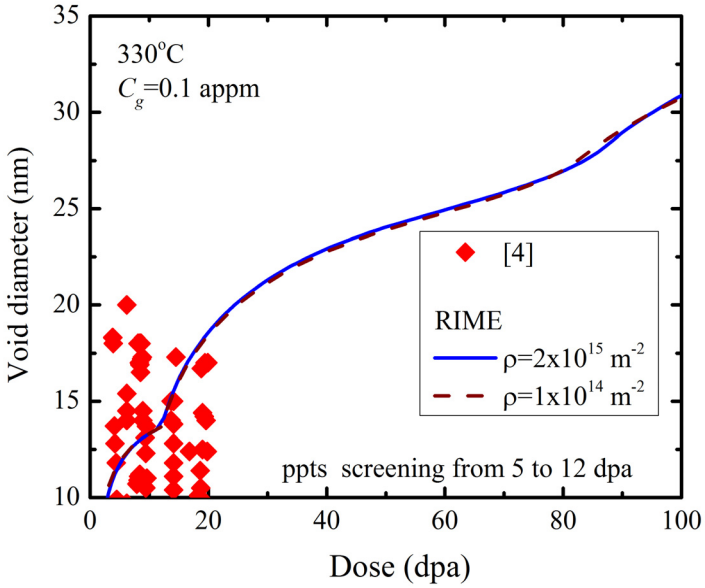

Fig. 20. Comparison of dose dependences of void size at 330°C calculated with the RIME code and measured in the temperature range of 315-335°C in [4].

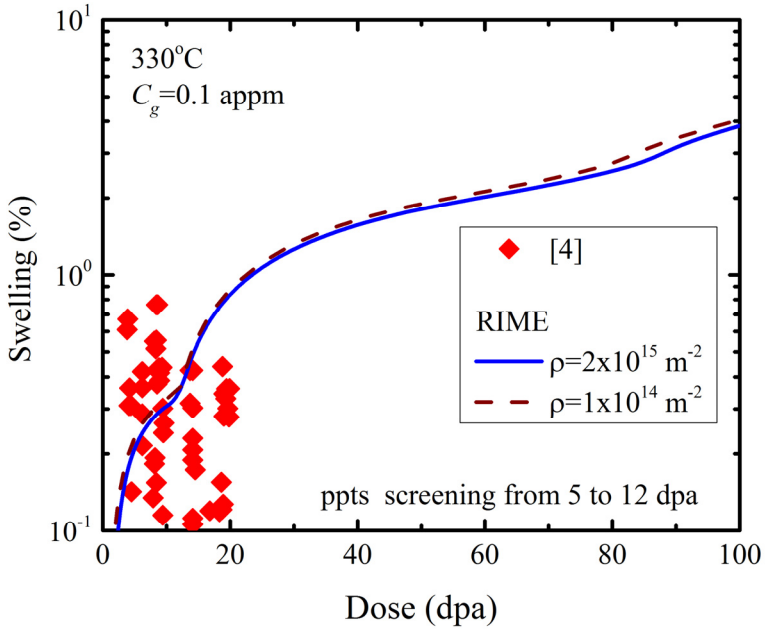

Fig. 21. Comparison of dose dependences of void size at 330°C calculated with the RIME code and measured in the temperature range of 302-315°C in [4].

The data for 370°C in [19] in Figs. 22 and 23 shows that swelling is larger as compared to those in [4], which is expected since the irradiation temperature is higher. Moreover, the data show a non-monotonic swelling behavior around 10 dpa, which is similar to that in our calculation results on Figs. 20 and 21, where the correlation between voids and ppts is taken into account. Using doses ϕ_1 and ϕ_2 in Eq. (9), equal to 5 and 12 dpa, respectively, resulted in a good correspondence between calculations and experimental data. Hence one may conclude that association of voids with ppts which screen voids from 1-D migrating SIA clusters takes place at the both temperatures, 330 and 370°C, in similar dose range. Note also that in the latter case swelling at high doses is of ~10%, which is quite close to that found in fast breeder reactor at 400°C.

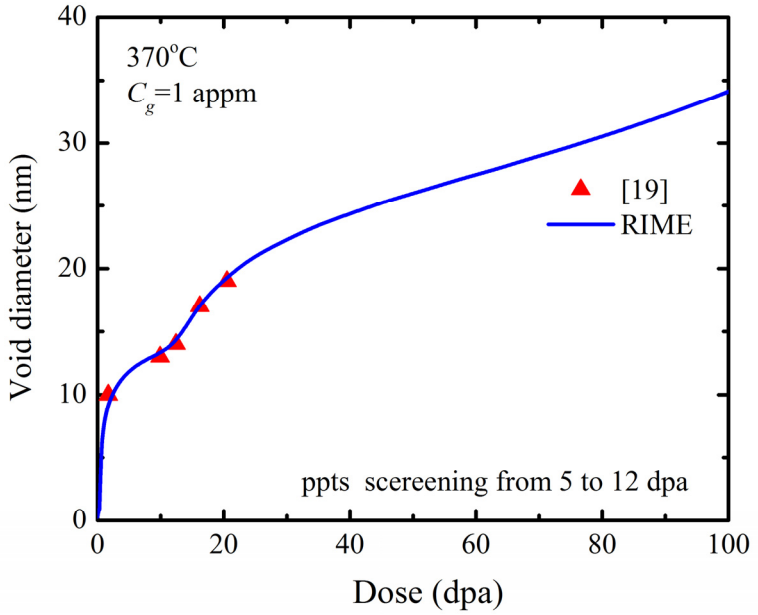

Fig. 22. Comparison of dose dependences of void size at 370°C calculated by RIME and measured in [19].

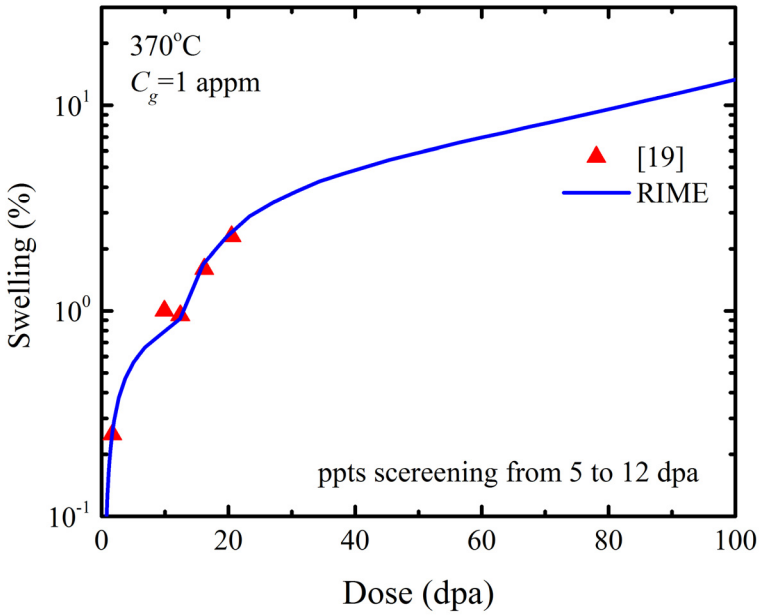

Fig. 23. Comparison of dose dependences of swelling at 370°C calculated by RIME and measured in [19].

4. Conclusions

Experimental data on swelling in stainless steels irradiated at LWR conditions have been analyzed by mean-field rate theory calculations, using the RIME code developed at ORNL, which accounts for correct nature of the primary defect production in displacement cascades during neutron irradiation and details of gas-assistant void nucleation. The following conclusions have been drawn.

1. The incubation period of swelling is not related to the difficulty in void nucleation, as usually thought; the voids form from the very beginning of irradiation, supported by residual gas atoms and large vacancy super-saturation.
2. Even small amounts of residual gas have profound effect on void nucleation, which diminish importance of He from transmutation reactions.
3. Small levels of swelling observed during incubation period are explained by saturation of void size due to large reaction cross-section with 1-D migrating SIA clusters in the absence of spatial correlations of voids with other defects.
4. Spatial correlations of voids with secondary phase particles leads to a twofold increase of saturation void size, which does not affect the picture significantly.
5. An increase of swelling rate during transient stage of swelling is due to development of spatial correlation between voids and dislocations, which are able to screen voids completely from migrating SIA clusters.

Importantly, it follows from the present work that decreasing residual gas concentration may provide a way to decrease swelling in reactor materials.

References

1. C. Cawthorne, and E.J. Fulton, "Voids in irradiated stainless steel," *Nature* 216 (1967) 575-576.
2. R. Bullough, B. L. Eyre, and K. Krishan, "Cascade damage effects on swelling of irradiated materials," *Proceedings of the Royal Society of London Series* A 346 (1975), 81-102.
3. S.J. Zinkle, P. Maziasz, and R.E. Stoller, "Dose dependence of the microstructural evolution in neutron-irradiated austenitic stainless steel," *J. Nucl. Mater*. 206 (1993), 266-286.
4. S.I. Porollo et al., "Determination of the Lower Temperature Limit of Void Swelling of Stainless Steels at PWR-Relevant Displacement Rates", *The Effects of Radiation on Materials, 21st International Symposium, ASTM STP1447,* M. L. Grossbeck, *T. R. Allen, R. G. Lott, and A. S. Kumar, Eds., ASTM International, West Conshohocken, PA, 2003.*
5. D.J. Edwards et al., "Influence of irradiation temperature and dose gradients of the microstructural evolution of neutron-irradiated 316SS," *J. Nucl. Mater.* 317 (2003), 32-45.
6. H.M. Chung, "Assessment of void swelling in austenitic stainless steel core internals," NUREG/CR-6897, ANL-04/28, Argonne National Laboratory, December 2004.
7. D.J. Edwards et al., "Nano-cavities observed in a 316SS PWR flux thimble tube irradiated to 33 and 70 dpa," *J. Nucl. Mater*. 384 (2009), 249-255.
8. L. Fournier et al., "Cluster dynamic prediction of the microstructure evolution of 300-series austenitic stainless steels under irradiation: Influence of helium," 15th Int. Conference on Environmental Degradation of Materials in Nuclear Power Systems-Water Reactors, J. T. Busby, G. Ilevbare, P. L. Andresen, Eds., August 7-1, 2011, Colorado Springs, Colorado, USA.
9. R.E. Stoller, A.V. Barashev, and S.I. Golubov, "Low-temperature Swelling in LWR Internal Components: Current Data and Modeling Assessment," Oak Ridge National Laboratory, ORNL/LTR-2012/390, 2012.
10. R.E. Stoller, A.V. Barashev, and S.I. Golubov, "The Influence of Helium on Low-temperature Swelling in LWR Internal Components," Oak Ridge National Laboratory, ORNL/LTR-2013/200, May 2013.
11. L. Fournier et al., "Cluster dynamic prediction of void swelling in austenitic stainless steals irradiated under PWR and FBR conditions," 16th International Conference on Environmental Degradation of Materials in Nuclear Power Systems-Water Reactors, August 11-15, 2013, Ashville, NC, USA.
12. R.E. Stoller, S.I. Golubov, and A.V. Barashev, **"**Low-temperature swelling in LWR internal components: a computational assessment," 17th International Conference on Environmental Degradation of Materials in Nuclear Power Systems – Water Reactors, Ottawa, Ontario, Canada, August 9-12, 2015.
13. R.E. Stoller, "Primary Radiation Damage Formation," in Comprehensive Nuclear Materials, R. J. M. Konings, T.R. Allen, R.E. Stoller, and S. Yamanaka, Eds., Elsevier Ltd., Amsterdam, 2012, pp. 293-332.

14. Kozlov, I.A. Portnykh, L.A. Skryabin, E.A. Kinev, Temperature effect on characteristics of void population formed in the austenitic steel under neutron irradiation up to high damage dose, Journal of Nuclear Materials 30 7–311 (2002) 956–960.
15. F. Garner, and D.S. Gelles, "Neutron-induced Swelling of Commercial Alloys at Very High Exposures," Effects of irradiation on materials: 14th Int. Symp. (V. II0 ASTM STP 1046, N.H.N. Packan, R.E. Stoller, and A.S. Kumar, Eds., American Society for Testing and Materials, Philadelphia, 1990, pp. 673-683.
16. A.V. Barashev, and S.I. Golubov, **"**Unlimited damage accumulation in metallic materials under cascade-damage conditions," *Philos. Mag*. 89 (2009), 2833-2860.
17. S.I. Golubov, A.V. Barashev, and R.E. Stoller, "Radiation Damage Theory," in Comprehensive Nuclear Materials, R.J.M. Konings, T.R. Allen, R.E. Stoller, and S. Yamanaka, Eds., Elsevier Ltd., Amsterdam, 2012, pp. 357-391.
18. B.N. Singh, A.J.E. Foreman, and H. Trinkaus, "Radiation hardening revisited: role of intra cascade clustering," *J. Nucl. Mater*. 249 (1997), 103-115.
19. E.N. Shcherbakov et al., Influence of damage rate on physical and mechanical properties and swelling of 18Cr–9Ni austenitic steel in the range of $3x10^{-9}$ to $4x10^{-8}$ dpa/s, *J. Nucl. Mat,* 386–388 (2009) 152–156.
20. A.V. Barashev, S.I. Golubov, and R.E. Stoller, "A Model of Radiation-induced Microstructural Evolution," Oak Ridge National Laboratory, ORNL Report ORNL/L TR-2014/487, 2014.
21. S.I. Golubov et al., "Grouping method for the approximate solution of a kinetic equation describing the evolution of point-defect clusters," *Philos. Mag*. A 81 (2001), 643-658.
22. S.I. Golubov, R.E. Stoller, and S.J. Zinkle, "An Improved Solution to the Kinetic Equations Describing Defect Cluster Dynamics During Irradiation or Thermal Ageing," GEN-IV Nuclear Energy System, ORNL-GEN4/LTR-06-012, 2006.
23. S.I. Golubov et al., "Kinetics of coarsening of helium bubbles during implantation and post-implantation annealing," *J. Nucl. Mater*. 361 (2007), 149-159.
24. N.F. Carnahan, and K.E. Starling, "Equation of State for Nonattracting Rigid Spheres," *J. Chem. Phys*. 51 (1969), 635-636.
25. R.E. Stoller, "Modeling Dislocation Evolution in Irradiated Alloys," *Met. Trans.* 21A (1990), 1829-1837.
26. S.I. Golubov, B.N. Singh, and H. Trinkaus, "On recoil-energy-dependent defect accumulation in pure copper. Part II. Theoretical treatment," *Philos. Mag. Series* A 81 (2001), 2533-2552.
27. S. J. Zinkle and F. A. Garner, "Effect of Initial Oxygen Content on the Void Swelling Behavior of Fast Neutron Irradiated Copper," *J. Nucl. Mater*., 329-333 (2004) 938-941.
28. Y. Shimomura, H. Mukoda, M. Kiritani, S. Kojima and F. A. Garner, "Experiments to Examine the Contribution of Gaseous Atoms on Void Formation in Irradiated Metals," *J. Nucl. Mater*., 212-215 (1994) 352-357.